Kinetic and Structural Evidence for the Importance of Tyr236 for the Integrity of the Mo Active Site in a Bacterial Sulfite Dehydrogenase †

ARTICLE *in* BIOCHEMISTRY · SEPTEMBER 2006

Impact Factor: 3.02 · DOI: 10.1021/bi060058b · Source: PubMed

8 AUTHORS, INCLUDING:

Changjian Feng
University of New Mexico
60 PUBLICATIONS **1,039** CITATIONS

SEE PROFILE

Kinetic and Structural Evidence for the Importance of Tyr236 for the Integrity of the Mo Active Site in a Bacterial Sulfite Dehydrogenase†

Ulrike Kappler,*,‡ Susan Bailey,§ Changjian Feng,|| Michael J. Honeychurch,‡ Graeme R. Hanson,⊥ Paul V. Bernhardt,‡ Gordon Tollin,# and John H. Enemark||

Centre for Metals in Biology, School of Molecular and Microbial Sciences, The University of Queensland, Brisbane, Qld 4072, Australia, CCLRC Daresbury Laboratory, Warrington WA4 4AD, U.K., Department of Chemistry, University of Arizona, Tucson, Arizona 85721, Centre for Magnetic Resonance, The University of Queensland, Brisbane, Qld 4072, Australia, and Department of Biochemistry and Molecular Biophysics, University of Arizona, Tucson, Arizona 85721

Received January 11, 2006; Revised Manuscript Received April 15, 2006

ABSTRACT: The sulfite dehydrogenase from *Starkeya novella* is the only known sulfite-oxidizing enzyme that forms a permanent heterodimeric complex between a molybdenum and a heme *c*-containing subunit and can be crystallized in an electron transfer competent conformation. Tyr236 is a highly conserved active site residue in sulfite oxidoreductases and has been shown to interact with a nearby arginine and a molybdenum−oxo ligand that is involved in catalysis. We have created a Tyr236 to Phe substitution in the SorAB sulfite dehydrogenase. The purified SDH^{Y236F} protein has been characterized in terms of activity, structure, intramolecular electron transfer, and EPR properties. The substituted protein exhibited reduced turnover rates and substrate affinity as well as an altered reactivity toward molecular oxygen as an electron acceptor. Following reduction by sulfite and unlike SDH^{WT}, the substituted enzyme was reoxidized quickly in the presence of molecular oxygen, a process reminiscent of the reactions of the sulfite oxidases. SDH^{Y236F} also exhibited the pH-dependent CW-EPR signals that are typically observed in vertebrate sulfite oxidases, allowing a direct link of CW-EPR properties to changes caused by a single-amino acid substitution. No quantifiable electron transfer was seen in laser flash photolysis experiments with SDH^{Y236F}. The crystal structure of SDH^{Y236F} clearly shows that as a result of the substitution the hydrogen bonding network surrounding the active site is disturbed, resulting in an increased mobility of the nearby arginine. These disruptions underline the importance of Tyr236 for the integrity of the substrate binding site and the optimal alignment of Arg55, which appears to be necessary for efficient electron transfer.

The oxidative detoxification of the highly reactive sulfite anion to the chemically inert sulfate is a reaction that is found in all domains of life and in organisms as diverse as plants, birds and higher animals, bacteria, and archaea. While the oxidation of sulfite may be linked to energy-generating respiratory processes in microorganisms and mitochondria (*1*−*3*), its main function appears to be a detoxification reaction in plants and especially mammals and birds, where high tissue concentrations of sulfite have been implicated in nerve cell damage (*4*) and the lack of a functional sulfite-oxidizing enzyme leads to severe developmental retardation and early death of affected individuals (*5*).

All sulfite-oxidizing enzymes that have been characterized to date belong to a subfamily of the mononuclear molybdenum enzymes, the sulfite oxidase (SO)[1] family. By far the best studied examples of such enzymes are the SOs isolated from mammalian and avian liver that have been studied since the late 1960s (*1*). The so-called sulfite oxidases differ from the sulfite dehydrogenases (SDHs) that are part of the same enzyme family in their ability to use molecular oxygen as an electron acceptor. This difference is reflected in the two distinct EC numbers given to these enzymes, EC 1.8.3.1 (SO) and EC 1.8.2.1 (SDH).

The crystal structure of chicken liver SO (CSO) was reported in 1997 (*6*), and more recently, the crystal structures of a plant SO from *Arabidopsis thaliana* (*7*) and that of a bacterial sulfite dehydrogenase (SDH) from *Starkeya novella* have been determined (*8*). All three enzymes share two central domains, the molybdenum domain and the dimerization domain, which adopt very similar folds in all cases. Despite the similarity of these central domains, however,

† This work was funded by a grant and fellowship to U.K. by The University of Queensland. P.V.B. gratefully acknowledges financial support of the Australian Research Council (Project DP0343405). Support by the National Institutes of Health (Grant GM 37773 to J.H.E.) is gratefully acknowledged.

* To whom correspondence should be addressed. Telephone: +61 7 3365 4093. Fax: +61 7 3365 4620. E-mail: u.kappler@uq.edu.au.

‡ Centre for Metals in Biology, School of Molecular and Microbial Sciences, The University of Queensland.

§ CCLRC Daresbury Laboratory.

|| Department of Chemistry, University of Arizona.

⊥ Centre for Magnetic Resonance, The University of Queensland.

Department of Biochemistry and Molecular Biophysics, University of Arizona.

[1] Abbreviations: CSO, chicken sulfite oxidase; CW-EPR, continuous wave EPR; dRF, deazariboflavin; EPR, electron paramagnetic resonance; HSO, human sulfite oxidase; IET, intramolecular electron transfer; *lpH*, low-pH; SDH, sulfite dehydrogenase; SO, sulfite oxidase; SDH, SorAB sulfite dehydrogenase; SDH^{WT}, wild-type SorAB sulfite dehydrogenase; SDH^{Y236F}, Y236F substituted SorAB sulfite dehydrogenase; WT, wild type.

10.1021/bi060058b CCC: $33.50
Published on Web 07/20/2006

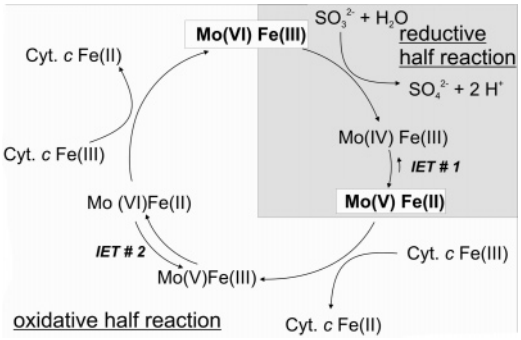

FIGURE 1: Schematic representation of the proposed sulfite oxidation mechanism in SO and SDH-like proteins.

significant differences in the overall structure of the three enzymes exist: while both the chicken liver and plant SO are homodimers (*7*, *9*) in which the dimerization domain mediates the contact between two identical subunits, the bacterial SDH (SDH^{WT}) does not exhibit this interaction. Instead, it is a heterodimer consisting of a large, molybdenum-binding subunit (SorA) and a small heme *c*-containing subunit (SorB) (*8*, *10*). The dimerization domain does not mediate the interactions between these two subunits, and its function in the bacterial enzyme is not immediately apparent. The heme content of the sulfite-oxidizing enzymes is another of their distinguishing features. While the plant SO lacks any heme-containing domains and/or subunits (*7*), chicken liver SO (CSO) contains a heme *b* binding domain connected to the central molybdenum/dimerization domain by a flexible linker region (*6*), and the bacterial SDH has the heterodimeric, heme *c*-containing structure outlined above (*8*).

In the crystal structure of chicken liver SO, the enzyme is found in an apparently inactive conformation where the heme *b* domain is located 32 Å from the molybdenum center, a position too remote to allow efficient interdomain electron transfer from the Mo site (*6*). In contrast, the heme and molybdenum centers of the bacterial SDH are in close proximity (Mo···Fe distance of ~16.6 Å), and thus, the crystal structure of this enzyme has for the first time allowed direct insights into potential electron transfer pathways between the two redox centres (*8*). Flash photolysis studies on the kinetics of intramolecular electron transfer (IET) between heme and molybdenum centers in the bacterial SDH demonstrate that the IET occurs directly through the protein medium (*11*). Intriguingly, the SorB subunit and the heme *b* domain of the CSO have a similar overall shape, and in CSO, the latter can be modeled in the position occupied by SorB in the SDH^{WT} structure with only minor steric hindrances (*8*). The bacterial SDH therefore is an ideal model for studying electron transfer pathways in sulfite-oxidizing enzymes without the complicating factor of domain movement.

The molybdenum center of both SOs and SDHs is the site of sulfite oxidation, leading to a two-electron reduction of this redox center [Mo(VI) to Mo(IV)] (Figure 1). These electrons are then passed on to an external electron acceptor either directly (plant enzyme) or via a heme group (human and chicken SO and bacterial SDH), which restores the molybdenum ion to its resting, hexavalent oxidation state. In the vertebrate and bacterial enzymes, the external acceptor molecule is itself a cytochrome that is linked to the respiratory chain.

The fully oxidized Mo(VI) center of the sulfite-oxidizing enzymes described to date has a square pyramidal coordination geometry in which the metal atom is coordinated by three equatorial S donors, namely, a bidentate dithiolene group of the molybdopterin cofactor and a conserved cysteine residue and two oxo ligands, which occupy an axial and an equatorial position. The equatorial oxo ligand is thought to be the target of a nucleophilic attack by the sulfite S atom and participates in a coupled two-electron oxygen atom transfer reaction. The equatorial oxo ligand is therefore crucial for the sulfite oxidation reaction.

A number of residues that are important in hydrogen bonding with the substrate and/or the molybdenum center have been identified on the basis of the three crystal structures and kinetic studies on mutant forms of the human sulfite oxidase (HSO) (*12*−*14*). One of these residues is a tyrosine that hydrogen bonds with the equatorial oxo ligand of the molybdenum center, the substrate, and a histidine residue. This tyrosine residue (Tyr343 in HSO, Tyr322 in CSO, and Tyr236 in SDH^{WT}) is conserved in sulfite-oxidizing enzymes and the related plant nitrate reductases. Kinetic studies of a Y343F substituted HSO (HSO^{Y343F}) revealed clear changes in k_{cat}, $K_{M\ sulfite}$, and $k_{cat}/K_{M\ sulfite}$, with k_{cat} reduced to ~35% of the wild-type HSO (HSO^{WT}) activity at pH 8.0 (*13*). In addition, non-steady-state parameters showed that the rate of the reductive half-reaction (k_{red}^{heme}, Figure 1) of HSO^{Y343F} was similar to steady-state k_{cat} measurements, and that the reductive half-reaction proceeded at only 2.5−20% of the k_{red}^{heme} observed in HSO^{WT} (*13*). This appears to be a result of changes in the rates of electron transfer between the two redox centers (*14*), while pre-steady-state experiments on the isolated molybdenum domain demonstrated that the rate of turnover of the Mo center alone remained high in both the wild-type and substituted HSO (*13*). These results show that the Y343F substitution causes changes in both the substrate binding properties of HSO and its ability to transfer electrons between the Mo and heme *b* redox centers; however, structural data for HSO, showing the underlying changes at a molecular level, are not available.

We have substituted Tyr236 of SorAB with a phenylalanine residue and characterized the substituted enzyme, SDH^{Y236F}. In this paper, we describe SDH^{Y236F} in terms of its structure, enzyme activity, electrochemically driven catalysis, intramolecular electron transfer (IET), and spectroscopic properties. The changes in catalytic activity are related to structural changes seen in the active site conformation of the substituted SDH.

EXPERIMENTAL PROCEDURES

Bacterial Strains and Growth Media. Escherichia coli strains were routinely cultivated in liquid or solid Luria-Bertani medium, and antibiotics were added to the medium when appropriate (*15*). *E. coli* strain DH5α (Invitrogen) was used for cloning and plasmid propagation, and strain S17-1 (*16*) was used for conjugative transfer of plasmids. *Rhodobacter capsulatus* 37B4 Δ*dorA* (*17*) and derivative strains carrying expression plasmids were cultivated on either TYS (*18*) or RCV (*19*) medium as described in ref *17*. For expression of the recombinant protein, the strains were grown anaerobically for 40−48 h under high light conditions in RCV medium containing 60 mM dimethyl sulfoxide (DMSO) and 1 mM sodium molybdate.

Kits and Reagent. Unless otherwise stated, all chemicals were analytical-grade. Kits for isolation of plasmid DNA were purchased from Sigma-Aldrich, and PCR purification and PCR gel extraction kits were from Qiagen. Cytochrome *c* (horse heart) for use in SDH assays was purchased from Sigma-Aldrich (catalog no. C-7752).

Generation of a Y236F Mutant of the SorAB Protein. Standard molecular biological methods were used throughout (*15*, *20*). A Y236F mutation was introduced into plasmid pSorex (*17*) using the Quikchange mutagenesis kit (Stratagene) and primers Y236Ffwd (TGG ATG AAG ACC GCC TTC CGC ATC CCG GAC AAT G) and Y236Frev (C ATT GTC CGG GAT GCG GAA GGC GGT CTT CAT CCA). PCR-based mutagenesis was carried out according to the manufacturer's instructions with the addition of 1% DMSO and an extension time of 7 min at 68 °C. The resulting clones were analyzed by DNA sequencing (BigDye version 3.1, Applied Biosystems), and plasmids carrying the desired mutation were designated pSorexY236F. The insert of pSorexY236F was then subcloned into the broad host-range vector pRK415 (*21*) and the resulting plasmid pRK-sorexY236F transferred into *R. capsulatus* 37B4 Δ*dorA* by conjugative transfer as described in ref *17*. Finally, the pRK-sorexY236F plasmid was re-isolated from the recombinant *R. capsulatus* strains and the mutation confirmed by DNA sequencing.

Purification of Recombinant Sulfite Dehydrogenase. Purification of recombinant SDH^{WT} and SDH^{Y236F} was carried out as described previously (*17*). Unless otherwise stated, all purification and centrifugation steps were carried out at 4 °C. Recombinant protein was purified from either periplasmic (*17*) or whole cell extracts. Whole cell extracts were prepared by resuspending cell pellets in an appropriate volume of 10 mM Tris-HCl buffer (pH 7.8) followed by two passages through a French pressure cell (Thermo Electron Corp.) at 14 000 psi. Cell debris was removed by centrifugation at 30000*g* for 30 min, and cell membranes were removed in a subsequent centrifugation at 145000*g* for 90 min in an L6-60 Beckman ultracentrifuge. Supernatants from this step were loaded directly onto a DEAE anion exchanger column, and the purification was carried out as described in ref *17*.

Crystallization and Solution of the SDH^{Y236F} Crystal Structure. Recombinant SDH^{Y236F} was crystallized as previously described (*22*), and crystals were cryo-cooled within 4 days of the crystallization trials being set up. Data were collected on beamline 14.2 of the SRS, Daresbury Laboratory. Data were processed and scaled using Mosflm/SCALA (*23*), and further analyses used programs from the CCP4 suite (*24*). The crystal structure was refined with REFMAC (*25*) using the native sulfite dehydrogenase model (*8*) (Protein Data Bank entry 2blf) as the starting point, and inspection of the model and electron density maps was carried out using O (*26*). Data collection, processing, and refinement statistics are given in Table 1. The final model comprises residues 1−373 of the SorA subunit, residues 1−81 of the SorB subunit, one molybdenum cofactor (Moco), one *c*-type heme, a sulfate ion, and water molecules. The structures have good stereochemistry with 99.5% of the residues in the most favored and additionally allowed regions and no residues in disallowed regions of the Ramachandran plot as defined by PROCHECK (*27*).

Table 1: Data Collection and Refinement Statistics

Data Collection	
beamline	SRS 14.2
wavelength (Å)	0.98
resolution range (Å)	50−1.8
no. of unique reflections	46488
completeness (%)[a]	96.8 (82.1)
multiplicity[a]	6.2 (4.0)
$I/\sigma(I)$[a]	14.5 (2.2)
R_{merge}[b] (%)[a]	11.0 (60.5)
Refinement	
resolution range (Å)	20−1.8
R_{cryst}[c] (%)	16.6
R_{free}[d] (%)	20.9
rms deviations from ideal geometry	
bond lengths (Å)	0.013
bond angles (deg)	1.4
no. of water molecules	424
average *B*-factor (Å^2)	
SorA atoms	16
SorB atoms	18
water atoms	26

[a] Values in parentheses refer to the highest-resolution shell (2.1−2.0 Å). [b] $R_{merge} = \sum_h\sum_i|(I_{hi} - I_h)|/\sum_h\sum_i(I_{hi})$. [c] $R_{cryst} = \sum|F_o - F_c|/\sum F_o$, where F_o and F_c are the observed and calculated structure factor amplitudes, respectively. [d] R_{free} was calculated with 5% of the data that had been excluded from refinement.

Weighted difference Fourier maps calculated with $mF_{obs} - DF_{calc}$ coefficients showed a strong negative peak on the molybdenum atom and suggested that this atom is not fully occupied. To help estimate the occupancy of the molybdenum, omit maps were calculated, with data from the substituted and wild-type protein, by setting the occupancy of selected atoms (molybdenum, equatorial and apical oxygen ligands, and all side chain atoms of Arg55, Cys104, and Phe236) to zero, followed by five cycles of refinement and calculation of weighted difference Fourier maps using $mF_{obs} - DF_{calc}$ coefficients. The electron density peak for the molybdenum atom in the omit maps was significantly lower for the data from SDH^{Y236F} than for the data from SDH^{WT} with fully occupied molybdenum at the same resolution, while the peak heights of the sulfur ligands were similar in both structures. The occupancy of the molybdenum was estimated to be 60%. Further refinement with the molybdenum occupancy set appropriately resulted in a reasonable *B*-factor for this atom, similar to that of surrounding atoms, and no significant residual difference density.

Biochemical Characterization of SDH^{Y236F}. Denaturing and nondenaturing polyacrylamide gels were prepared according to the method of ref *28* and used to assess the purity of protein preparations. In-gel stains for the sulfite-oxidizing enzyme activity following native PAGE at 4 °C were carried out as described in ref *29*. The molybdenum content of the recombinant sulfite dehydrogenase was analyzed by ICP-MS at the ACQUIRE center at The University of Queensland using protein samples that had been intermittently stored at −80 °C. Analytical ultracentrifugation was carried out as described in ref *17*. Heme content was determined by the method described in ref *30*. Protein concentrations were determined using the 2D-Quant kit (GE Healthcare). Sulfite dehydrogenase activity assays were routinely carried out at 25 °C in 20 mM Tris-acetate buffer (pH 8.0) in the presence of 2 mM sodium sulfite and 0.04 mM cytochrome *c* (horse heart). In some cases, the cytochrome *c* was replaced with 1

mM potassium ferricyanide. A Hitachi U-3000 split-beam spectrophotometer equipped with a thermostated cell holder was used to monitor the reaction at 550 nm (cytochrome *c*) or 420 nm (ferricyanide). Extinction coefficients of 21.1 mM^{-1} cm^{-1} (550 nm) for cytochrome *c* and 1.02 mM^{-1} cm^{-1} (420 nm) for potassium ferricyanide were used to compute enzyme activities. k_{cat} values are reported as the number of sulfite molecules oxidized per second. Assay buffers were titrated with glacial acetic acid (*10*, *31*). Sodium sulfite stock solutions (from 200 to 0.2 mM) were prepared freshly each day in 50 mM Tris-HCl (pH 8.8) and 5 mM EDTA, and cytochrome stock solutions (2 mM) were prepared daily in 20 mM Tris-acetate (pH 8.0). For the determination of a pH profile, SorAB activity assays were carried out in 50 mM Tris-acetate buffers titrated to the desired pH. The higher buffer concentration was chosen to compensate for the reduced buffering ability of Tris at the extremes of the pH range that was tested. The pH of the assay mixtures was checked before and after the enzymatic reaction. Determination of K_M values for sulfite was carried out in either 20 mM Bis-Tris-acetate (pH 6.0) or 20 mM Tris-acetate (pH 8.0). Sulfite concentrations were varied between 0.1 and 300 μM (from 0.5 to 100 μM for SDH^{Y236F}) at pH 6.0 and between 1 and 500 μM (from 6 to 2000 μM for SDH^{Y236F}) at pH 8.0. K_M values for cytochrome *c* were determined using an Applied Photophysics SX.18MV stopped-flow apparatus to overcome limitations imposed by the 1 cm light path of the spectrophotometer. Final concentrations of 20 mM buffer and 2 mM sulfite were used in these experiments, and cytochrome *c* concentrations were varied between 0.6 and 40 μM. Catalytic constants were determined by direct nonlinear fitting of the data to the Michaelis−Menten equation. Data relating to the pH dependence of the SorAB activity were fitted to eq 1 using Sigma Plot version 9.0 (Systat Software Inc.).

$$y = \frac{V_{\max\ \lim}}{1 + 10^{pK_a - pH} + 10^{pH - pK_b}} \quad (1)$$

The reactivity of SDH^{WT} and SDH^{Y236F} toward oxygen was studied by recording the changes in absorption spectra (240−650 nm) of a 2.5 μM enzyme solution reduced with 50 μM sodium sulfite over an extended period of time. Oxygen electrode experiments were carried out at 30 °C using a Hansatech Oxygraph 1.1 device according to the manufacturer's instructions.

Catalytic Voltammetry of SDH^{WT} and SDH^{Y236F}. Both SDH^{WT} and SDH^{Y236F} sulfite dehydrogenases were immobilized on a graphite electrode using 100 μM enzyme solutions as described previously (*32*). The edge plane surface of the graphite electrode was freshly cleaved with a microtome, sonicated in Millipore water, and allowed to dry. A pipetting solution was made by mixing 2.0 μL of 5 mg/mL polylysine, 0.5 μL of 50 mM Tris-HCl (pH 8.0), and 1.0 μL of a 100 μM enzyme solution; 1.5 μL of this solution was pipetted onto the electrode surface and allowed to dry overnight in a refrigerator at 5 °C. Experiments were performed in 50 mM Tris-HCl buffer containing approximately 250 μM sulfite. The pH of the solution in the electrochemical cell was adjusted by the addition of OH^-. Additional experiments were performed using Tris-acetate buffers and 2.4 mM sulfite.

Laser Flash Photolysis Studies. Laser flash photolysis experiments were performed anaerobically on 0.50 mL of solutions containing 5-deazariboflavin (dRF) and 0.5 mM freshly prepared semicarbazide as the sacrificial reductant. The dRF solution was de-aerated when it was vigorously bubbled with H_2O-saturated O_2-free argon for at least 2 h, and argon was purged over the surface of the protein solution to remove traces of O_2 before the protein droplet was mixed into the bulk solution. Experiments were performed at room temperature.

Electron Paramagnetic Resonance. EPR samples were prepared in buffers containing 100 mM Bis-Tris, 100 mM NaCl (pH 7.0, low pH), or 100 mM Bis-Tris propane (pH 9.5, high pH). The pH was adjusted by adding HCl. One milligram of protein was reduced with a 20-fold excess of sodium sulfite and immediately frozen in liquid nitrogen. The continuous wave EPR spectra were recorded on a Bruker ESR-300E spectrometer at 77 K.

EPR redox potentiometric titrations were performed with a Bruker Elexsys E580 X-band EPR spectrometer. Mo(V) spectra were recorded at 130 K (modulation amplitude of 2.0 G and microwave power of 20 mW). Titrations were performed in a Belle Technology anaerobic box (<10 ppm O_2) in a constantly stirred temperature-controlled cuvette. The enzyme concentration was 50 μM in a 50 mM tricine buffer (pH 8.0). To stabilize the solution potential, a mixture of transition metal mediators (*33*) was employed: Fe(tcta), $[Fe(tacn)_2]Br_3$, $[Co\{(NME_3)_2sar\}]Cl_5$, $[Co(ClMEN_5Ssar)]Cl_3$, $[Co(AMMEN_4S_2sar)]Cl_3$, and $[Co(sep)]Cl_3$ all at concentrations of 20 μM. The titrants were $Na_2S_2O_4$ and $K_2S_2O_8$ (both at ∼5 mM). Potentials were measured with a homemade electrode comprising a Pt wire attached to a Ag/AgCl reference electrode, and this was calibrated with a pH 7 solution of quinhydrone. All potentials are cited versus the normal hydrogen electrode (NHE). All samples were transferred as 300 μL aliquots into an EPR tube in the anaerobic box, and the tube was sealed with a rubber septum. The EPR tube was removed from the glovebox and immediately frozen in liquid nitrogen. The intensity of the middle *g* value [$I(E)$] was taken to be proportional to the concentration of Mo^V in the sample, and this was fitted to a modified form of the Nernst equation (eq 2) describing consecutive one-electron reductions (redox potentials E_1 and E_2) that generate an EPR active intermediate with maximum intensity I_{max}.

$$I(E) = \frac{I_{max}}{1 + 10^{(E - E_1)/59} + 10^{(E_2 - E)/59}} \quad (2)$$

Deposition. The coordinates of the SDH^{Y236F} structure have been deposited with the Protein Data Bank as entry 2C9X.

RESULTS

Biochemical Characterization of SDH^{Y236F}. The SDH^{Y236F} *S. novella* sulfite dehydrogenase could be purified to homogeneity as described previously (*17*). The molybdenum content of the purified, substituted enzyme was 1.08 atoms of Mo/holoenzyme, and alkaline hemochrome spectra revealed a heme content of 0.75 heme group/holoenzyme. These values indicate that, as isolated, SDH^{Y236F} contained a full complement of both redox cofactors and that storage

Table 2: Steady-State Kinetic Parameters of the SDH^{WT} Sulfite Dehydrogenase and the SDH^{Y236F} Sulfite Dehydrogenase at pH 6.0 and 8.0 in Comparison to Corresponding Values Obtained for Vertebrate Sulfite Oxidases[a]

	$K_{M\ app\ sulfite}$ (μM)	k_{cat} (s^{-1})	$k_{cat}/K_{M\ app\ sulfite}$ ($M^{-1}\ s^{-1}$)	$K_{M\ app\ cyt\ c}$ (μM)	$k_{cat}/K_{M\ app\ cyt\ c}$ ($M^{-1}\ s^{-1}$)	ref
			pH 8.0			
wild-type SDH	21.8 ± 2.6	333.7 ± 10.5[b]	1.53×10^7	2.2 ± 0.2	1.52×10^8	this work
Y236F SDH	114 ± 13.5	52.51 ± 1.6	4.61×10^5	0.4 ± 0.02	1.31×10^8	this work
wild-type chicken SO	16.4 ± 3	95.0 ± 1.9	5.78×10^6	2.2 ± 0.5	4.30×10^7	*31*
wild-type human SO	4.35 ± 0.11	25.9 ± 0.17	5.97×10^6	nd	nd	*13*
Y343F human SO	17.6 ± 0.5	8.59 ± 0.03	4.89×10^5	nr	nr	*13*
			pH 6.0			
wild-type SDH	0.4 ± 0.1	33.51 ± 1.47	8.13×10^7	4.4 ± 0.3	7.62×10^6	this work
Y236F SDH	4.3 ± 0.6	36.19 ± 1.54	8.42×10^6	0.5 ± 0.04	7.24×10^8	this work
wild-type chicken SO	10.2 ± 0.98	16.6 ± 0.38	1.63×10^6	2.2 ± 0.2	7.50×10^6	*31*
wild-type human SO	1.29 ± 0.3	13.2 ± 0.35	1.05×10^7	nd	nd	*13*
Y343F human SO	8.68 ± 0.14	3.11 ± 0.03	3.59×10^5	nr	nr	*13*

[a] Errors given for sulfite dehydrogenase activities represent standard errors. [b] Previously published k_{cat} values in ref *17* were reported as turnovers per minute.

of the protein at −80 °C did not cause a significant loss of molybdenum.

After nondenaturing PAGE, purified SDH^{Y236F} exhibited a single band that migrated to the same position as SDH^{WT} and could be stained for sulfite oxidizing activity (data not shown). Using analytical ultracentrifugation, a single protein species of 43 kDa was detected, a value that compares well with the values of 42 and 42.6 kDa reported previously for the native and recombinant SDH^{WT} protein, respectively (*17*). Both findings show that the Y236F substitution did not cause a change in the subunit composition of the enzyme.

The kinetic parameters of sulfite oxidation for both the substituted and the wild-type enzyme were determined at pH 8.0 in 20 mM Tris-acetate buffer and at pH 6.0 in 20 mM Bis-Tris-acetate buffer. The former pH was chosen because it is in the region of maximal SDH^{WT} activity and the latter because pH 6.0 is a pH value at which the intramolecular electron transfer rate can be measured for the SDH^{WT} protein (*11*). Previously reported kinetic parameters for SDH^{WT} (*17*) had been determined in Tris-HCl buffers that may cause inhibition of sulfite oxidation in this type of enzyme, and therefore, the properties of SDH^{WT} were redetermined using the new buffer system. The results of the kinetic investigation of the two proteins are summarized in Table 2 and clearly show the inhibitory influence of the chloride anions on enzyme activity: the previously determined k_{cat} values for SDH^{WT} (*17*) correspond to only ~60% of the activity measured here using Tris-acetate buffers.

At pH 8.0, the apparent K_M for sulfite was approximately 5 times higher for SDH^{Y236F} and the apparent k_{cat} was reduced to ~16% of the SDH^{WT} value (Table 2). Thus, the apparent second-order constant $k_{cat}/K_{M\ sulfite}$ is reduced by 2 orders of magnitude in SDH^{Y236F} under these assay conditions. Unexpectedly, SDH^{Y236F} exhibited a higher affinity for cytochrome *c*, with an apparent $K_{M\ cyt\ c}$ of 0.4 μM, approximately 5 times smaller than that of SDH^{WT} (Table 2).

At pH 6.0, both SDH^{WT} and SDH^{Y236F} had a higher affinity for sulfite than at pH 8.0, but the relative difference between the apparent $K_{M\ sulfite}$ values of SDH^{WT} and SDH^{Y236F} was even greater than at pH 8.0 ($K_{M\ sulfite}$ for SDH^{Y236F} equals only ~10% of the SDH^{WT} value at pH 6.0). The difference in the affinities for cytochrome *c* also increased to a factor of ~10, with the substituted enzyme retaining the higher affinity. In contrast, the apparent k_{cat} values of the two enzymes are very similar at pH 6.0 (33.5 s^{-1} for SDH^{WT}, ~10% of the activity at pH 8.0, and 36.19 s^{-1} for SDH^{Y236F}, ~70% of the activity observed at pH 8.0). This is in contrast to what Wilson and co-workers found for HSO, where the substituted HSO^{Y343F} enzyme consistently exhibited a lower activity (33 and 23% at pH 8.0 and 6.0, respectively) than HSO^{WT}, and both proteins had similar apparent $K_{M\ cyt\ c}$ values (4.4 and 5.1 μM, respectively) at pH 8.5 (*13*).

Dependence of Sulfite Oxidizing Activity on pH. For both SDH^{WT} and SDH^{Y236F}, the pH dependence of the sulfite oxidizing activity was determined and the data were fitted to eq 1 which describes a bell shape. While for SDH^{WT} a maximum of sulfite oxidizing activity clearly exists at pH 8.5, the activity profile of the SDH^{Y236F} protein exhibited little variation of the sulfite oxidizing activity between pH 6.0 and 8.5. The fit of the data to eq 1 predicts pK_a values of 7.6 and 9.4 for SDH^{WT} and 5.5 and 9.5 for SDH^{Y236F} using cytochrome *c* as the electron acceptor (Figure 2A). Ferricyanide can be used as an alternative electron acceptor in SO/SDH assays, and it has been shown for mammalian and avian SOs that ferricyanide can interact directly with the molybdenum center of these enzymes (*1*). To test whether SDH^{Y236F} activity might be influenced by the choice of electron acceptor, an activity versus pH profile for SDH^{Y236F} was determined using ferricyanide as the electron acceptor (Figure 2B). It was found to be very similar to the one previously obtained (Figure 2A); however, it exhibited only a single pK_a value of 9.5 (Figure 2B).

Direct Voltammetry of SDH^{WT} and SDH^{Y236F}. The results from the standard steady-state activity determinations described above were further confirmed after immobilization of both enzymes on an edge plane pyrolytic graphite electrode. In the presence of sulfite, the catalytic current was determined over a pH range of 5.5−9.4 in 50 mM Tris-HCl buffers. While the results for SDH^{WT} were very similar to those previously obtained (*32*), the activity of SDH^{Y236F} was severely reduced and could only be observed between pH 7.2 and 8.64 (Figure 2C).

With the exception of the highest pH that was used, the measurements of the SDH^{Y236F} catalytic current were very similar (0.11 μA ± 10%). At pH 7.9, the SDH^{Y236F} catalytic current corresponded to approximately 12% of the activity of the immobilized SDH^{WT}, confirming the differences in activity observed at pH 8.0 in solution assays. The electro-

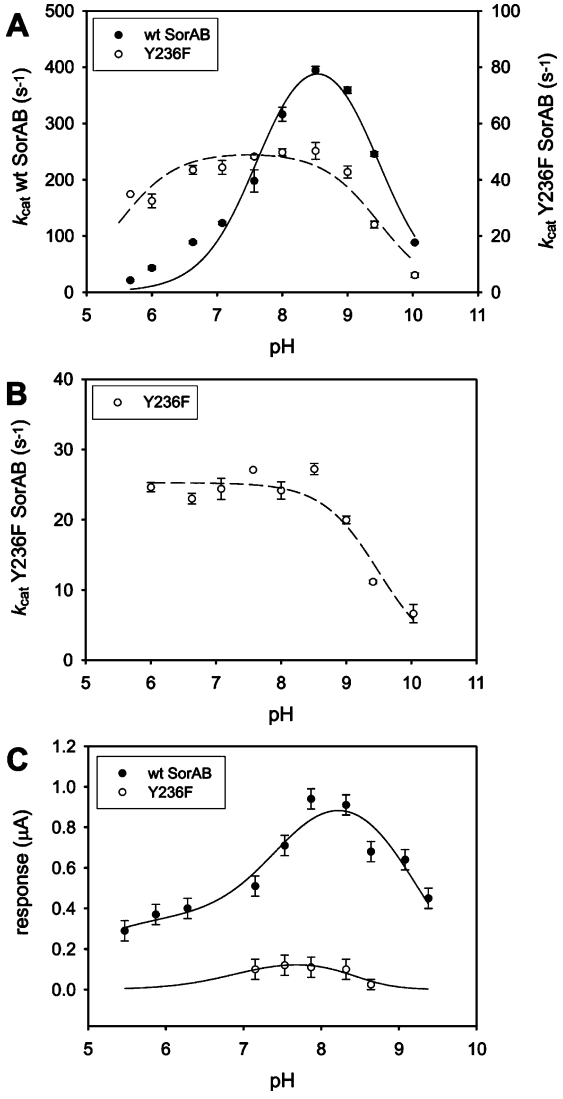

FIGURE 2: pH dependence of sulfite oxidizing activity in SDH^{WT} and SDH^{Y236F}. (A) Sulfite oxidizing activity of SDH^{WT} and SDH^{Y236F} in 50 mM Tris-acetate buffers using cytochrome *c* as an electron acceptor. (B) Sulfite oxidizing activity of SDH^{Y236F} in 50 mM Tris-acetate buffer using ferricyanide as an electron acceptor. (C) Sulfite oxidizing activity of SDH^{WT} and SDH^{Y236F} immobilized on a graphite electrode: (●) SDH^{WT} and (○) SDH^{Y236F}. Data points in panels A and B are averages of three activity determinations, and the standard error is indicated.

chemical turnover of both SDH^{WT} and SDH^{Y236F} was pH-dependent. At pH 7.87, E_{cat} was 244 mV for SDH^{WT} and 237 mV for SDH^{Y236F}. Within the experimental error, no significant differences in the E_{cat} values for the two enzymes were observed for the pH range that was investigated.

Reactivity of SDH^{Y236F} toward Oxygen. In contrast to SDH^{WT}, SDH^{Y236F} was found to be readily reoxidized by oxygen following reduction with a 20-fold excess of sulfite as judged by the spectrum of the SorB heme *c* group (Figure 3). This reoxidation occurred with an average rate of 0.35 μM/min at pH 8.0, while SDH^{WT} exhibited little sign of reoxidation for at least 50−60 min under the same conditions followed by slow reoxidation at an average rate of 0.038 μM/min at pH 8.0. Attempts to further quantify this "sulfite oxidase" activity of SDH^{Y236F} using an oxygen electrode failed, however, probably due to the relatively low levels of activity.

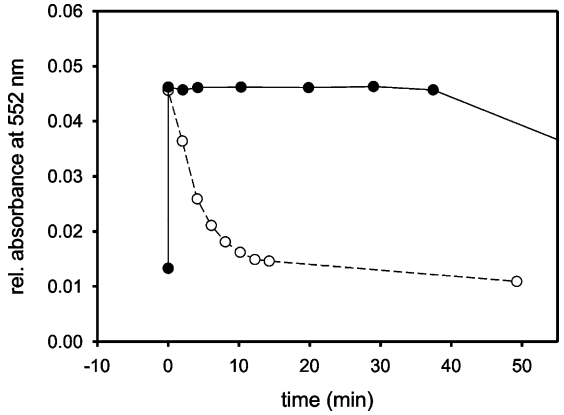

FIGURE 3: Reoxidation of SDH^{WT} and SDH^{Y236F} by oxygen at pH 8.0. Samples contained 2.5 μM protein and were reduced with 50 μM sulfite. The first data point represents the absorbance prior to sulfite reduction: (●) SDH^{WT} and (○) SDH^{Y236F}. The normalized absorbance changes at 552 nm (α-band peak) are shown.

Intramolecular Electron Transfer As Measured by Laser Flash Photolysis. Efficient transfer of electrons between the two redox centers of a SO or a SDH is essential for the sulfite oxidation reaction to proceed. Two IET events have to occur during the proposed mechanism of sulfite oxidation (Figure 1), and the second IET between the oxidized heme and a one-electron-reduced Mo center [Mo(V)] can be measured in the reverse direction [i.e., from Fe(II) to Mo(VI)] by laser flash photolysis in the presence of deazariboflavin (dRF) (*12*). The method involves reduction of the heme group of the fully oxidized [Mo(VI)Fe(III)] enzyme by a dRF radical under anaerobic conditions and determination of the electron transfer rate (Fe → Mo) by following the decay of the ferrous heme optical absorption at 553 nm. IET rates for SDH^{WT} can only be determined at pH 6.0, and there the IET process is reversible between the Mo(VI)Fe(II) and Mo(V)Fe(III) forms, allowing determination of the kinetic and equilibrium constants (*11*).

The same experiment with SDH^{Y236F} at pH 6.0 and 5.8 showed a fast initial increase in the absorbance due to ferrous heme formation (as a result of heme reduction by $dRFH^{\bullet}$), but this was followed by virtually no decay of the 553 nm absorption band (data not shown), precluding determination of the overall IET rate and equilibrium constants.

Electron Paramagnetic Resonance Studies. SDH^{WT} is the first sulfite-oxidizing molybdenum enzyme to exhibit EPR spectra that are independent of pH and anions in the medium (*10*). Variable-frequency pulsed EPR studies of SDH^{WT} clearly show couplings from nearby exchangeable protons that are assigned to a Mo(V)-OH_n group (*34*). The hyperfine parameters for these exchangeable protons of SDH^{WT} are the same at both low and high pH and similar to those for the high-pH forms of SOs from eukaryotes.

In contrast, the CW-EPR spectra of SDH^{Y236F} (Figure 4) show a distinct dependence upon pH. The spectrum at low pH has all the properties of a typical low-pH (*lpH*) SO EPR spectrum. Note that the splittings in the H_2O buffer (cf. trace 1 in Figure 4) collapse in D_2O buffer (cf. trace 2 in Figure 4), indicating a nearby, solvent-exchangeable proton, similar to the *lpH* form of vertebrate SOs. The appearance of the high-pH EPR spectrum of SDH^{Y236F} is similar to those of SDH^{WT} and the high-pH form of SO from vertebrates; however, the principal *g* values for the high-pH spectrum of

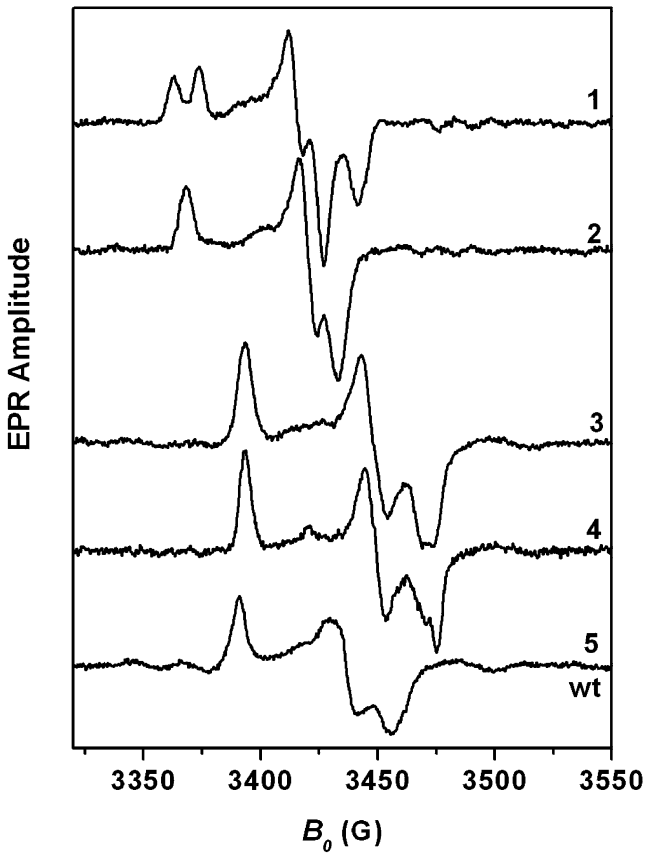

FIGURE 4: CW-EPR spectra of SorAB^{Y236F}: trace 1, pH 7.0 in H_2O (principal *g* values of 2.004, 1.973, and 1.965); trace 2, pD 6.6 in D_2O (buffers: 100 mM Bis-Tris, 100 mM NaCl); trace 3, pH 9.5 in H_2O (principal *g* values of 1.989, 1.957, and 1.944); and trace 4, pD 9.1 in D_2O (buffer: 100 mM Bis-Tris propane). The pH was adjusted with HCl (H_2O buffer) or DCl (D_2O buffer). EPR parameters: microwave frequency, 9.445 GHz; modulation amplitude, 1 G; microwave power, 200 μW; temperature, 77 K. Trace 5 is the CW-EPR spectrum of SorAB^{wt} at pH 9.5. Note that the wild-type EPR spectrum at pH 7.0 is the same as that at pH 9.5 (*10*).

SDH^{Y236F} (1.989, 1.957, and 1.944) are somewhat different from those for SDH^{WT} and vertebrate SO-type enzymes, for which these *g* values are essentially identical (1.990, 1.966, and 1.954).

EPR potentiometry was used to determine the redox potentials (pH 8.0) of the molybdenum center in both SDH^{WT} and SDH^{Y236F} (data not shown). For SDH^{WT}, the potentials were 160 ± 20 mV for the Mo(VI/V) couple and −49 ± 20 mV (both vs NHE) for the Mo(V/IV) couple. For SDH^{Y236F}, the values were 174 ± 20 and −23 ± 20 mV (vs NHE), respectively.

Crystal Structure of SDH^{Y236F}. The structure of SDH^{Y236F} confirms that Tyr236 has been substituted with a phenylalanine. The phenylalanine side chain of SDH^{Y236F} is in the same position as the tyrosine side chain of SDH^{WT}; however, the absence of the hydroxyl group results in the loss of key interactions. In SDH^{WT} (*8*) (Figure 5A), the OH group of Tyr236 is involved in hydrogen bond interactions with the equatorial hydroxo/water ligand to the Mo, His57 NE2, and a nearby water molecule; additionally, it is in close contact with S1′ of the molybdopterin cofactor, Arg55 NH2, and Arg55 NE. We also note that the side chain of the homologous Tyr322 residue in CSO (*6*) has been shown to hydrogen bond to the product sulfate which would displace the water molecule interaction observed in SDH^{WT} (*8*).

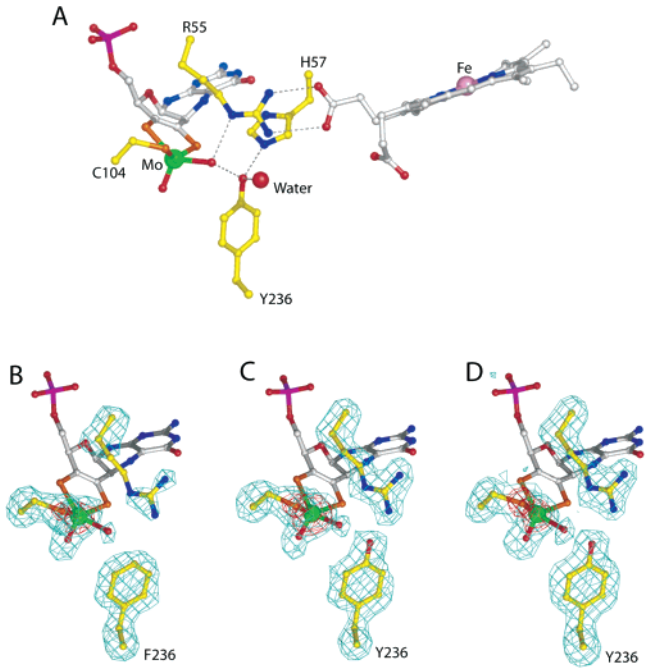

FIGURE 5: Active site structure of SDH^{WT} and SDH^{Y236F}. (A) The Moco and heme cofactors are shown together with residues Tyr236, Arg55, Cys104, and His57 which are grouped on one side of the sulfite/sulfate binding site. Hydrogen bond interactions with an atom−atom distance of less than 3.5 Å are shown as dashed lines and reveal the central role played by Tyr236. (B−D) Views of the molybdenum center of SDH^{Y236F} (B) and SDH^{WT} (C and D) enzymes showing electron density from omit maps calculated as described in Experimental Procedures and contoured at 2.6σ (cyan) and 10σ (red). The SDH^{WT} structure and omit map shown in panel D are from a redox-damaged form which has only 50% molybdenum present so that differences can be ascribed to the Y236F substitution rather than the loss of molybdenum. Atoms are colored according to type: green for molybdenum, pink for iron, orange for sulfur, magenta for phosphorus, red for oxygen, blue for nitrogen, white for Moco and heme carbon atoms, and yellow for side chain carbon atoms.

The absence of these close contacts in SDH^{Y236F} appears to lead to a less rigid active site. Figure 5 compares the calculated difference omit maps around the affected atoms for SDH^{Y236F} (Figure 5B) and SDH^{WT} (Figure 5C,D) crystal structures. The poor electron density and the high *B*-factors for the side chain of Arg55 in SDH^{Y236F} (Figure 5B) indicate disorder in the position of this residue, and this contrasts with the well-defined electron density in SDH^{WT}. In addition, there has been a partial loss of molybdenum during the crystallization process. The molybdenum−ligand bond distances of SDH^{Y236F} are similar to those of SDH^{WT} with the exception of the bond to Sγ of Cys104, which has increased slightly in length to 2.7 Å. The small apparent movement of the Cys104 side chain probably reflects the partial molybdenum loss and has been previously observed in a structure of SDH^{WT} crystallized in the presence of sulfite which also exhibited loss of molybdenum (Figure 5; U. Kappler and S. Bailey, unpublished results).

DISCUSSION

This is the first study of a substitution of the conserved the active site tyrosine residue in a sulfite-oxidizing enzyme

in which both kinetic properties and a complete crystal structure containing all redox centers of the substituted enzyme are reported.

The data presented above confirm that, as in the SOs, the active site tyrosine 236 (Tyr322 CSO and Tyr343 HSO) plays a crucial role in catalysis in the SorAB sulfite dehydrogenase. This clearly manifests itself in the changes to the kinetic constants of SDH^{Y236F} relative to the SDH^{WT} (Table 2) (*13*, *14*).

At pH 8.0, close to the pH optimum for catalysis, the kinetic data obtained for wild-type SorAB, CSO, and HSO enzymes exhibit overall similarities. However, it is striking that at this pH, the k_{cat} for SDH^{WT} is 3.5 times greater than that of the CSO^{WT} (*31*) and almost 13 times larger than the value for HSO^{WT} (*13*) (Table 2). This is very likely a consequence of the different quaternary structure of the bacterial enzyme, in which the two redox centers remain in proximity and poised for efficient IET at all times. As a consequence, k_{cat}/K_M (the specificity constant, or the apparent second-order rate constant at low substrate concentrations) for the bacterial SDH^{WT} protein is also approximately 2.6 times larger than that of its vertebrate counterparts. At pH 8.0, the K_M for the sulfite of SDH^{WT} is slightly higher than the corresponding values for the vertebrate SOs, a feature that is often observed in enzymes with increased turnover rates.

When the kinetic parameters at pH 8.0 are compared with those obtained at pH 6.0 (Table 2), it becomes apparent that SDH^{WT} behaves like HSO^{WT} (*13*); in both enzymes, k_{cat}/K_M increases at the lower pH value (Table 2). The k_{cat}/K_M values of HSO^{Y343F} and SDH^{Y236F}, however, behave differently; for HSO^{Y343F}, the second-order rate constant decreases slightly at pH 6.0, whereas the SDH^{Y236F} protein, like SDH^{WT}, shows an increase in the second-order rate constant at pH 6.0. The increase in the k_{cat}/K_M value for SDH^{Y236F} at pH 6.0 relative to its pH 8.0 value is 3.4 times greater than the corresponding increase seen for SDH^{WT}. Clearly, the lower pH value helps to overcome some of the functional limitations imposed by the Y236F substitution, as is illustrated by the nearly equal k_{cat} values for SDH^{WT} and SDH^{Y236F}.

Differences in reaction mechanism details (e.g., the necessity of domain movement in HSO) may account to some extent for the differing pH profiles obtained for SDH^{Y236F} and HSO^{Y343F}. For SDH^{Y236F}, all pH profiles clearly show that there is a marked loss of activity above pH 8.5 and that the activity remains constant at almost all other pH values that were tested. It had been suggested earlier that the high-pH pK_a value at pH ~9.4 seen in SDH^{WT} may be controlled by the formation of a Tyr236 phenolate anion (*32*), but this is clearly not the case as this pK_a value remains almost unchanged in SDH^{Y236F}. This then raises the question of how the high-pH pK_a value is controlled, and we suggest that it may be influenced by Arg55 that is also found close to the molybdenum center. For the lower-pH pK_a value which in SDH^{Y236F} shifts by at least 2 pH units toward the acidic range, this change may reflect an alteration of the substrate specificity of SDH^{Y236F} as in SDH^{WT} this pK_a coincides with the pK_a for the protonation of the substrate molecule to HSO_3^{2-} (*32*).

The effect of the Y236F substitution on the pH profile of SorAB clearly differs from what has been observed for HSO. The pH profiles of both HSO^{WT} and HSO^{Y343F} were shown to be dependent on buffer concentration, exhibiting a sigmoidal shape with a single low-pH pK_a in 20 mM buffer and a bell shape that could be fitted to two pK_a values in 100 mM buffers (*13*). Independent of buffer strength, the low-pH pK_a shifted to a more basic pH in HSO^{Y343F}, while this pK_a was shifted toward the acidic in SDH^{Y236F}.

The changes of sulfite oxidizing activity with pH clearly demonstrate that although HSO (for which no crystal structure is currently available), CSO, and SorAB likely have very similar active site geometries and structures, they are dissimilar in some aspects of their kinetic behavior, and these may be directly related to differences in the residues surrounding the active site, for example, Ala358/Arg450/Arg472 or Ser105/Ala186/Ala208 (SorAB, CSO, and HSO numbering, respectively), or due to the requirement for cytochrome domain movement and docking in the vertebrate SOs.

In the SDH^{WT} structure, the Tyr236 side chain plays an important role in the substrate binding site where it forms a hydrogen bond to the equatorial oxygen ligand of the molybdenum and is well placed to interact with bound sulfite. In the CSO structure, the equivalent residue, Tyr322, hydrogen bonds to bound sulfate at the active site (*6*). The Y236F substitution removes a potential hydrogen bond to the substrate and/or product which correlates well with the observed 5−10-fold increase in the K_M for sulfite. We observed some dissociation of molybdenum during crystallization of SDH^{Y236F}, which appears to be correlated with the long time scale for crystallization (data were collected 4 days after crystallizations were set up), whereas SDH^{WT} crystallized at the same time with the same solutions remained intact. Therefore, we suggest that Tyr236 plays a crucial role in the stability of the catalytic center, and this is presumably mediated by interactions with the equatorial oxygen ligand of the molybdenum atom, with Arg55, and with His57. The question of whether the disordered Arg55 side chain and the slight change to the Cys104 position are due to the Y236F substitution or a consequence of reduced molybdenum occupancy arises. Fortunately, a SDH^{WT} structure obtained after crystallization in the presence of sulfite also exhibits reduced molybdenum occupancy and provides a convincing answer. There was no effect on the side chain of Arg55 in this wild-type structure (Figure 5D), so we believe that the disorder of this side chain is a direct consequence of the Y236F substitution. However, in the case of Cys104, the longer distance to the molybdenum appears to be caused by movement of the cysteine side chain rather than movement of the metal and is probably a consequence of the reduced molybdenum content, since a similar distance was also observed in SDH^{WT} crystallized in the presence of sulfite (ref *8* and unpublished data).

Arg55 has been shown to play a role in substrate and/or product binding (*6*), and given their positions, it is likely that both Tyr236 and Arg55 are involved in stabilization of the transition-state complex of the enzyme. The effect of the Y236F mutation on Arg55 demonstrates that interaction with Tyr236 and with the equatorial oxygen is necessary for ordered positioning of the arginine side chain, and this effect will contribute to the increase in $K_{M\ sulfite}$ and the reduced activity of SDH^{Y236F}. In addition, Arg55 forms a salt bridge with the heme propionate in SDH^{WT}, and disorder of Arg55 will reduce the strength of this interaction which could then reduce IET rates. Thus, our structure helps to explain the

important role that Tyr236 plays in substrate binding, IET, and the overall reactivity of the enzyme toward sulfite by picturing the disturbances caused at the molybdenum active site in the absence of this residue. However, the SDH^{Y236F} structure does not explain why the substituted enzyme exhibits a greater affinity for its electron acceptor, cytochrome *c*.

Our laser flash photolysis experiments showed that although SDH^{Y236F} is active at pH 6.0, no significant IET from Fe(II) to the Mo center occurred. Note that the laser flash photolysis technique follows the IET process in the reverse direction of the enzymatic turnover. The absence of quantifiable IET for SDH^{Y236F}, which is catalytically competent, is intriguing and could arise from either thermodynamic or kinetic factors. The Fe(III/II) redox potential of the six-coordinate heme site is expected to be relatively insensitive to the Y236F substitution, and this is indicated by the unchanged E_{cat} values seen in the protein film voltammetry experiments. Interestingly, the loss of the hydrogen bond interaction between the Mo center and the Tyr hydroxyl in SDH^{Y236F} did not have a marked influence on the Mo(VI/V) or Mo(V/IV) redox potentials. It is therefore unlikely that the observed effects of the Y236F substitution on SDH activity are a result of a change in the redox properties of the molybdenum center.

Another possibility is that the altered proton environment about the molybdenum center affects the electronic coupling between the Mo(VI/V) and Fe(III/II) centers and thereby changes the kinetics of IET. A recent theoretical paper indicates that aqueous tunneling pathways for electron transfer between redox cofactors in two separate protein domains are highly dependent on the structure of the intervening water molecules at their interface (*35*). The overall structure of the water molecules in the interface between the heme and molybdenum domains appears to be similar for SDH^{WT} and SDH^{Y236F}. However, the ~12 Å distance between the two redox cofactors falls within the range where the structure of the intervening water molecules is predicted to have a marked effect on electron tunneling pathways (*35*). It will therefore be important to study other mutants of SDH^{WT} to learn more about their influence on electron transfer pathways between the heme and Mo centers. Both Tyr236 and Arg55 are located on putative electron transfer pathways, and further studies, e.g., on mutations of the Arg55 residue and double mutations of both Arg55 and Tyr236, will be necessary to determine their respective roles in IET processes.

SDH^{Y236F} is a sulfite-oxidizing enzyme with more than one unusual property. In addition to being able to transfer electrons to molecular oxygen, SDH^{Y236F} also possesses changed EPR properties. In the SDH^{WT} enzyme, the EPR spectrum is independent of pH and anion concentration and resembles that of the "high-pH" conformation of the vertebrate SOs, while for the SDH^{Y236F} protein, both the high- and low-pH CW-EPR signal were observed. It would then seem that the changed SDH^{Y236F} EPR properties are due to the increased disorder observed at the Mo active site where the disruption of the extensive hydrogen bond network connecting the redox centers allows the molybdenum center to adopt a low-pH conformation. However, there most likely exist other, more subtle changes to the molybdenum redox center that can govern the high- to low-pH transitions of the SO/SDH molybdenum centers, since no disordered residues were reported for the CSO active site, although in this protein both CW-EPR signals are readily observed. The ability of a SO/SDH enzyme to transfer electrons to oxygen may be linked to the factors governing the high- to low-pH transition of the CW-EPR spectra.

In summary, our results clearly show for the first time the marked effect that a perturbation of the hydrogen bonding network surrounding the molybdenum active site, brought about by a Y236F substitution, has on spectroscopic and electron transfer properties of the SorAB SDH. Further investigations, especially into the factors influencing the reactivity of SDH^{Y236F} toward molecular oxygen and its EPR properties, will need to be undertaken in the future. Moreover, the unique structure of the SorAB SDH in which the two redox centers present in the enzyme are always in an electron transfer competent conformation allows direct insights into the effects of mutations on IET in SOs and SDHs that will be invaluable for furthering understanding of the underlying mechanisms.

ACKNOWLEDGMENT

We thank Dr. Andrei Astashkin for recording the EPR spectra.

REFERENCES

1. Rajagopalan, K. V. (1980) Sulfite oxidase (Sulfite:Ferricytochrome C Oxidoreductase), in *Molybdenum and Molybdenum-Containing Enzymes* (Coughlan, M. P., Ed.) pp 243−272, Pergamon Press, Oxford, U.K.
2. Myers, J. D., and Kelly, D. J. (2005) A sulphite respiration system in the chemoheterotrophic human pathogen *Campylobacter jejuni*, *Microbiology 151*, 233−242.
3. Yamanaka, T., Yoshioka, T., and Kimura, K. (1981) Purification of sulphite cytochrome *c* reductase of *Thiobacillus novellus* and reconstitution of its sulphite oxidase system with the purified constituents, *Plant Cell Physiol. 22*, 613−622.
4. Zhang, X., Vincent, A. S., Halliwell, B., and Wong, K. P. (2004) A mechanism of sulfite neurotoxicity: Direct inhibition of glutamate dehydrogenase, *J. Biol. Chem. 279*, 43035−43045.
5. Johnson, J. L., Rajagopalan, K. V., Renier, W. O., Van der Burgt, I., and Ruitenbeek, W. (2002) Isolated sulfite oxidase deficiency: Mutation analysis and DNA-based prenatal diagnosis, *Prenatal Diagn. 22*, 433−436.
6. Kisker, C., Schindelin, H., Pacheco, A., Wehbi, W. A., Garrett, R. M., Rajagopalan, K. V., Enemark, J. H., and Rees, D. C. (1997) Molecular basis of sulfite oxidase deficiency from the structure of sulfite oxidase, *Cell 91*, 973−983.
7. Schrader, N., Fischer, K., Theis, K., Mendel, R. R., Schwarz, G., and Kisker, C. (2003) The crystal structure of plant sulfite oxidase provides insights into sulfite oxidation in plants and animals, *Structure 11*, 1251−1263.
8. Kappler, U., and Bailey, S. (2005) Molecular basis of intramolecular electron transfer in sulfite-oxidizing enzymes is revealed by high-resolution structure of a heterodimeric complex of the catalytic molybdopterin subunit and a *c*-type cytochrome subunit, *J. Biol. Chem. 280*, 24999−25007.
9. Schindelin, H., Kisker, C., Hilton, J., Rajagopalan, K. V., and Rees, D. C. (1996) Crystal structure of DMSO reductase: Redox-linked changes in molybdopterin coordination, *Science 272*, 1615−1621.
10. Kappler, U., Bennett, B., Rethmeier, J., Schwarz, G., Deutzmann, R., McEwan, A. G., and Dahl, C. (2000) Sulfite:Cytochrome *c* Oxidoreductase from *Thiobacillus novellus*: Purification, characterization and molecular biology of a heterodimeric member of the sulfite oxidase family, *J. Biol. Chem. 275*, 13202−13212.
11. Feng, C. J., Kappler, U., Tollin, G., and Enemark, J. E. (2003) Laser-flash photolysis of a bacterial sulfite dehydrogenase, *J. Am. Chem. Soc. 125*, 14696−14697.
12. Feng, C. J., Wilson, H. L., Hurley, J. K., Hazzard, J. T., Tollin, G., Rajagopalan, K. V., and Enemark, J. H. (2003) Essential role

of conserved arginine 160 in intramolecular electron transfer in human sulfite oxidase, *Biochemistry 42*, 12235−12242.
13. Wilson, H. L., and Rajagopalan, K. V. (2004) The role of tyrosine 343 in substrate binding and catalysis by human sulfite oxidase, *J. Biol. Chem. 279*, 15105−15113.
14. Feng, C. J., Wilson, H. L., Hurley, J. K., Hazzard, J. T., Tollin, G., Rajagopalan, K. V., and Enemark, J. H. (2003) Role of conserved tyrosine 343 in intramolecular electron transfer in human sulfite oxidase, *J. Biol. Chem. 278*, 2913−2920.
15. Sambrook, J., Fritsch, E. F., and Maniatis, T. (1989) in *Molecular Cloning: A Laboratory Manual* (Ford, N., and Nolan, C., Eds.) Cold Spring Harbor Laboratory Press, Plainview, NY.
16. Simon, R., Priefer, U., and Puhler, A. (1983) A broad-host range mobilization system for in vivo engineering: Transposon mutagenesis in Gram-negative bacteria, *Bio/Technology 1*, 784−791.
17. Kappler, U., and McEwan, A. G. (2002) A system for the heterologous expression of complex redox proteins in *Rhodobacter capsulatus*: Characterization of recombinant sulfite:cytochrome *c* oxidoreductase from *Starkeya novella*, *FEBS Lett. 529*, 208−214.
18. Beringer, J. E. (1974) R factor transfer in *Rhizobium leguminosarum*, *J. Gen. Microbiol. 84*, 188−198.
19. Weaver, P. F., Wall, J. D., and Gest, H. (1975) Characterization of *Rhodopseudomonas capsulata*, *Arch. Microbiol. 105*, 207−216.
20. Ausubel, F. M., Brent, R., Kingston, R. E., Moore, D. D., Seidman, J. G., Smith, J. A., and Struhl, K. (2005) in *Current Protocols in Molecular Biology*, John Wiley & Sons Inc., Hoboken, NJ.
21. Keen, N. T., Tamaki, S., Kobayashi, D., and Trollinger, D. (1988) Improved broad-host-range plasmids for DNA cloning in Gram-negative bacteria, *Gene 70*, 191−197.
22. Kappler, U., and Bailey, S. (2004) Crystallization and preliminary X-ray analysis of sulfite dehydrogenase from *Starkeya novella*, *Acta Crystallogr. D60*, 2070−2072.
23. Otwinowski, Z., and Minor, W. (1997) Processing of X-ray Diffraction Data Collected in Oscillation Mode, *Methods Enzymol. 276*, 307−326.
24. CCP4 (1994) Collaborative Computational Project 4, *Acta Crystallogr. D10*, 760−763.
25. Murshudov, G. N., Vagin, A. A., and Dodson, E. J. (1997) Refinement of macromolecular structures by the maximum-likelihood method, *Acta Crystallogr. 53*, 240−255.
26. Jones, T. A., Zou, J. Y., Cowan, S. W., and Kjeldgaard, M. (1991) Improved methods for building protein models in electron density maps and the location of errors in these models, *Acta Crystallogr. A47*, 110−119.
27. Laskowski, R. A., Macarthur, M. W., Moss, D. S., and Thornton, J. M. (1993) Procheck: A Program to Check the Stereochemical Quality of Protein Structures, *J. Appl. Crystallogr. 26*, 283−291.
28. Laemmli, U. K. (1970) Cleavage of structural protein during the assembly of the head of bacteriophage T4, *Nature 227*, 680−685.
29. Cohen, H. J., and Fridovich, I. (1971) Hepatic Sulfite Oxidase: The nature and function of the heme prosthetic group, *J. Biol. Chem. 246*, 367−373.
30. Berry, E. A., and Trumpower, B. L. (1987) Simultaneous Determination of Hemes *a*, *b* and *c* from Pyridine Hemochrome Spectra, *Anal. Biochem. 161*, 1−15.
31. Brody, M. S., and Hille, R. (1999) The kinetic behavior of chicken liver sulfite oxidase, *Biochemistry 38*, 6668−6677.
32. Aguey-Zinsou, K. F., Bernhardt, P. V., Kappler, U., and McEwan, A. G. (2003) Direct electrochemistry of a bacterial sulfite dehydrogenase, *J. Am. Chem. Soc. 125*, 530−535.
33. Bernhardt, P. V., Chen, K.-I., and Sharpe, P. C. (2006) Transition metal complexes as mediator-titrants in protein redox potentiometry, *J. Inorg. Biochem. II* (in press).
34. Raitsimring, A. M., Kappler, U., Feng, C. J., Astashkin, A. V., and Enemark, J. H. (2005) Pulsed EPR studies of a bacterial sulfite-oxidizing enzyme with pH invariant hyperfine interactions from exchangeable protons, *Inorg. Chem. 44*, 7283−7285.
35. Lin, J., Balabin, I. A., and Beratan, D. N. (2005) The Nature of Aqueous Tunneling Pathways Between Electron-Transfer Proteins, *Science 310*, 1311−1313.

BI060058B